Eur. J. Mech. B/Fluids 18 (1999) 1005–1026

Spiral thermocapillary flows in two-layer systems

A.A. Nepomnyashchy [a,b], I.B. Simanovskii [a,*], L.M. Braverman [c]

[a] *Department of Mathematics, Technion—Israel Institute of Technology, 32000 Haifa, Israel*
[b] *Minerva Center for Nonlinear Physics of Complex Systems, Technion—Israel Institute of Technology, 32000 Haifa, Israel*
[c] *Department of Computer Science, Carmiel ORT College, Carmiel, Israel*

(Received 28 May 1998; revised 23 February 1999; accepted 25 March 1999)

Abstract – Parallel thermocapillary flows in infinite layers can be calculated easily. However, in reality thermocapillary flows occur in channels or closed cavities, and they are three-dimensional. In the present paper, a two-layer fluid system filling a channel with a rectangular cross section is considered. A numerical investigation of three-dimensional spiral thermocapillary flows generated by a temperature gradient imposed along the channel has been performed. Both the case of a zero longitudinal pressure gradient (a through flow in the channel) and that of a zero longitudinal fluid flux (a flow in the closed cavity) are investigated. Steady and oscillatory thermocapillary motions, and transitions between them are studied. © 1999 Éditions scientifiques et médicales Elsevier SAS

1. Introduction

The problem of a thermocapillary flow in an open liquid layer heated along the free surface is the subject of many investigations. The steady parallel flow in an infinite horizontal layer can be easily calculated (Levich [1], Birikh [2]). It is necessary to distinguish between two kinds of thermocapillary flows. If the flow occurs in a channel that connects two vessels kept under the same pressure, the mean longitudinal pressure gradient in the system is zero. The corresponding thermocapillary flow is usually called "linear flow" (Davis [3]). In the case of a closed cavity, the mean longitudinal flux of fluid is zero, so that a "return flow" occurs which is characterized by a non-zero longitudinal pressure gradient. The regimes of a two-dimensional secondary convection in a layer of a finite length were investigated numerically (see Ben Hadid and Roux [4,5]) and references therein). The above mentioned theoretical papers were based on a 'one-layer' approach: the hydrodynamic and heat processes in the gas phase were neglected, and a model condition for the temperature on the free surface was used. However, the dynamics of the gas phase can play an important role, and a 'two-layer' approach, when all the processes are considered simultaneously in both phases, would be more reliable. Such an approach is also necessary for the consideration of convection in the system of two immiscible liquid layers, as used, e.g. in the liquid encapsulation crystal growth technique. A thermocapillary parallel flow in a two-layer system was studied by Doi and Koster [6]. Numerical simulations of two-dimensional thermocapillary flows in closed cavities filled with two fluids were performed by Nepomnyashchy and Simanovskii [7], Simanovskii and Nepomnyashchy [8], Doi and Koster [6].

The two-dimensional computations deal with an idealized situation where the region is infinite in the horizontal transverse direction, and the fields of temperature, velocity and pressure are independent of the corresponding spatial variable. In reality, a cavity is finite in both directions transverse to the direction of

* Correspondence and reprints

the imposed temperature gradient. This circumstance leads to an inevitable appearance of three-dimensional flows. Let us consider, for instance, an infinitely long channel with a finite cross section. The boundaries of the channel are rigid and heated along the longitudinal direction. The velocity of the thermocapillary flow, and hence, the longitudinal convective heat transfer, vanish on the rigid boundaries. Therefore, the temperature in each cross section is higher in the middle of the channel than at its periphery. The horizontal temperature gradient induced by the boundaries generates a thermocapillary motion in the cross plane, in addition to the longitudinal thermocapillary flow. Thus, a fluid particle moves along the channel and simultaneously rotates in the transverse direction, so that the trajectory of the fluid particle is a spiral. We shall call such flows 'spiral flows'.

Thus, thermocapillary flows in a channel are 'three-dimensional'. They cannot be calculated analytically, and their computation can be done only by a special numerical analysis.

In the present paper, a two-layer fluid system filling a channel with a rectangular cross section is considered. We have performed a numerical investigation of three-dimensional stationary and non-stationary spiral thermocapillary flows generated by the imposed longitudinal temperature gradient. Steady secondary thermocapillary motions, within the rigid boundaries, have been calculated. Both cases of the linear and return flows are considered. The spiral flows stability problem is also discussed.

2. Formulation of the problem and the numerical method

Let us consider a long channel $-l_x/2 < x < l_x/2,\ -l/2 < y < l/2,\ -a_2 < z < a_1$ filled with two immiscible viscous fluids (see *figure 1*). Density, kinematic and dynamic viscosities, heat conductivity and thermal diffusivity of the i-th fluid ($i = 1, 2$) are $\rho_i, \nu_i, \eta_i, \kappa_i, \chi_i$ respectively. The thickness of the i-th layer is a_i. The temperature on the horizontal rigid boundaries $z = a_1$ and $z = -a_2$ is fixed in the following way: $T = Ax$, where A is the constant longitudinal temperature gradient. The vertical rigid boundaries $y = \pm l/2$ are thermally insulated. The interfacial tension σ decreases linearly with temperature: $\sigma = \sigma_0 - \alpha T$. The buoyancy force is neglected.

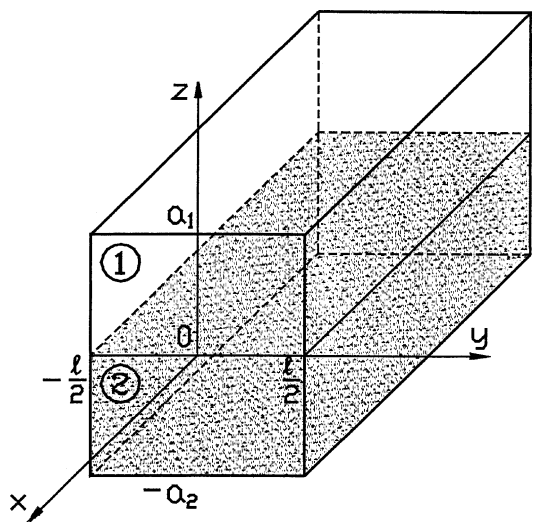

Figure 1. Geometrical configuration of the region and coordinate axes. The origin O is within the front cross-section.

In the present paper the interface is assumed to be plane: $z = 0$. This assumption is quite natural in the case of the linear flow, i.e. in the absence of the pressure gradient along the interface. In the case of the return flow, this assumption needs some explanation. The interface can be perfectly flat only if longitudinal pressure gradients appearing in both fluids are equal. Generally, these gradients are not equal, so that the interface is deformed in such a way that the pressure difference generated by the thermocapillary motion is balanced by the hydrostatic pressure and the interfacial tension. However, in some cases the deformation is negligible. The relevant parameters characterizing the interface deformation are $\epsilon = Al_x\alpha/\sigma_0$ (Pshenichnikov and Tokmenina [9]) and $R = Al_x\alpha/(\rho_2 - \rho_1)ga_2$ (Tan et al. [10]); g is the acceleration due to gravity. In the present paper, we assume that these parameters are small, hence the interface deformation caused by the difference of longitudinal pressure gradients can be neglected.

Obviously, under the assumption $z = 0$ we disregard the deformational instabilities discovered by Smith and Davis [11]. One can expect these instabilities to be unimportant if the crispation numbers $C_j = \eta_j\chi_j/a_j\sigma_0 \ll 1$, and the Galileo numbers $G_j = ga_j^3/\nu_j\chi_j \gg 1$, $j = 1, 2$.

The following notations are used: $\rho = \rho_1/\rho_2$, $\nu = \nu_1/\nu_2$, $\eta = \eta_1/\eta_2$, $\kappa = \kappa_1/\kappa_2$, $\chi = \chi_1/\chi_2$, $a = a_2/a_1$. As the units of length, time, velocity, pressure and temperature, a_1, a_1^2/ν_1, ν_1/a_1, $\rho_1\nu_1^2/a_1^2$ and Aa_1 are used, respectively.

The complete system of nonlinear equations can be written in the following dimensionless form:

$$\frac{\partial \mathbf{v}_1}{\partial t} + (\mathbf{v}_1 \cdot \nabla)\mathbf{v}_1 = -\nabla p_1 + \Delta \mathbf{v}_1, \qquad \frac{\partial T_1}{\partial t} + \mathbf{v}_1 \cdot \nabla T_1 = \frac{1}{P}\Delta T_1, \quad \nabla \cdot \mathbf{v}_1 = 0; \tag{1}$$

$$\frac{\partial \mathbf{v}_2}{\partial t} + (\mathbf{v}_2 \cdot \nabla)\mathbf{v}_2 = -\rho\nabla p_2 + \frac{1}{\nu}\Delta \mathbf{v}_2, \qquad \frac{\partial T_2}{\partial t} + \mathbf{v}_2 \cdot \nabla T_2 = \frac{1}{\chi P}\Delta T_2, \quad \nabla \cdot \mathbf{v}_2 = 0, \tag{2}$$

where $P = \nu_1/\chi_1$ is the Prandtl number.

On the rigid horizontal plates, the following boundary conditions are used:

$$z = 1: \quad \mathbf{v}_1 = 0, \ T_1 = x; \tag{3}$$

$$z = -a: \quad \mathbf{v}_2 = 0, \ T_2 = x. \tag{4}$$

At the interface, the normal components of the velocity vanish:

$$z = 0: \quad v_{z1} = v_{z2} = 0; \tag{5}$$

and the continuity conditions are fulfilled for the tangential components of the velocity

$$z = 0: \quad v_{x1} = v_{x2}, \ v_{y1} = v_{y2}, \tag{6}$$

for the tangential stresses

$$z = 0: \quad \eta\frac{\partial v_{x1}}{\partial z} = \frac{\partial v_{x2}}{\partial z} + \frac{M\eta}{P}\frac{\partial T_1}{\partial x}, \ \eta\frac{\partial v_{y1}}{\partial z} = \frac{\partial v_{y2}}{\partial z} + \frac{M\eta}{P}\frac{\partial T_1}{\partial y}, \tag{7}$$

for the temperature

$$T_1 = T_2; \tag{8}$$

and for the heat fluxes

$$\kappa\frac{\partial T_1}{\partial z} = \frac{\partial T_2}{\partial z}. \tag{9}$$

The lateral boundaries are rigid and thermally insulated:

$$y = \pm L/2: \quad \mathbf{v}_i = 0, \ \frac{\partial T_i}{\partial y} = 0. \tag{10}$$

Here $M = \alpha A a_1^2/\eta_1\chi_1$ is the Marangoni number, and $L = l/a_1$.

We consider the limit $l_x \to \infty$ and disregard the boundary conditions at $x = \pm l_x$. In this case, it is necessary to impose some additional conditions determining the pressure gradients in the system. In the case of a linear flow, the mean longitudinal pressure gradient in the system vanishes. In the case of a return flow, there is no mean longitudinal flux of fluids, so that

$$\int_{-L/2}^{L/2} dy \int_0^1 dz\, v_{x1} = 0, \qquad \int_{-L/2}^{L/2} dy \int_{-a}^0 dz\, v_{x2} = 0 \tag{11}$$

for any x. In the present paper, both cases are considered.

In the absence of rigid lateral boundaries ($L \to \infty$), the boundary value problem (1)–(10) has an exact solution corresponding to a parallel flow in the direction opposite to the direction of the temperature gradient:

$$\mathbf{v}_i = U_i(z)\mathbf{e}_x, \qquad p_i = B_i x, \qquad T_i = x + \Theta_i(z), \quad i = 1, 2,$$

where $\mathbf{e}_x$ is the unit vector of the axis x (Doi and Koster [6]). In the case of the zero longitudinal pressure gradient (linear flow),

$$U_1(z) = \frac{a\eta M}{P(1+a\eta)}(z-1), \tag{12}$$

$$U_2(z) = -\frac{\eta M}{P(1+a\eta)}(z+a); \tag{13}$$

$$\Theta_1(z) = \frac{a\eta M}{6(1+a\eta)}\left[(z-1)^3 - \frac{1+2\chi a^2+3\kappa a}{1+\kappa a}(z-1)\right], \tag{14}$$

$$\Theta_2(z) = \frac{\eta M}{6(1+a\eta)}\left[-\chi(z+a)^3 + \frac{a(\chi\kappa a^2+2\kappa+3\chi a)}{1+\kappa a}(z+a)\right]; \tag{15}$$

$$B_1 = B_2 = 0. \tag{16}$$

Note that the deviations of the temperature $\Theta_i(z) \leqslant 0$ in this case. In the case of the zero longitudinal fluxes of fluids (return flow),

$$U_1(z) = \frac{a\eta M(-1+4z-3z^2)}{4P(1+a\eta)}, \tag{17}$$

$$U_2(z) = -\frac{\eta M(a^2+4az+3z^2)}{4aP(1+a\eta)}; \tag{18}$$

$$\Theta_1(z) = \frac{a\eta M(1-z)[a(a\chi+\kappa)+(1+a\kappa)(z-5z^2+3z^3)]}{48(1+a\eta)(1+a\kappa)}, \tag{19}$$

$$\Theta_2(z) = \frac{\eta M(a+z)[a^2(a\chi+\kappa)-\chi(1+a\kappa)(a^2z+5az^2+3z^3)]}{48a(1+a\eta)(1+a\kappa)}; \tag{20}$$

$$B_1 = -\frac{3a\eta M}{2(1+a\eta)P}, \tag{21}$$

$$B_2 = -\frac{3M}{2aP(1+a\eta)}; \tag{22}$$

An example of the velocity and temperature profiles is shown in *figure 2* (see below for the details). Near the interface, the flow is directed opposite to the temperature gradient, whereas near the rigid boundaries the direction of the flow and that of the temperature gradient coincide. The established profiles of the temperature deviations $\Theta_i(z)$ result from the competition between the heat transfer by a "warm" flow near the interface and a "cold" flow near the boundaries. Using the expressions (19) and (20), we find that the temperature deviation at the interface is always positive. From the expressions for the temperature gradients

$$\frac{d\Theta_1}{dz} = \frac{a\eta M}{48(1+a\eta)(1+a\kappa)}\left[1-\chi a^2 - 12(1+a\kappa)z(1-z)^2\right], \quad 0 \leqslant z \leqslant 1,$$

$$\frac{d\Theta_2}{dz} = \frac{\eta M}{48a(1+a\eta)(1+a\kappa)}\left[\kappa a^2(1-\chi a^2) - 12\chi(1+a\kappa)z(z+a)^2\right], \qquad -a \leqslant z \leqslant 0,$$

in the case $1-\chi a^2 < 0$, one finds that $\Theta_1(z) \geqslant 0$ in the whole region $0 \leqslant z \leqslant 1$, while $\Theta_2(z)$ is negative in a certain region near the lower rigid boundary. Similarly, in the case $1-\chi a^2 > 0$, we find that $\Theta_2(z) \geqslant 0$ in the whole region $-a \leqslant z \leqslant 0$, while $\Theta_1(z)$ is negative in a certain region near the upper rigid boundary. If $1-\chi a^2 = 0$, both functions $\Theta_1(z)$ and $\Theta_2(z)$ are non-negative in the regions of their definition.

Near the rigid lateral boundaries $y = \pm L/2$, the flow is dragged due to the boundary condition (10). The longitudinal velocities $v_{xi} = U_i,\ i = 1, 2$, therefore necessarily depend on both transverse coordinates y and z. It is natural to expect that the field $|U_i(y, z)|$ has its maximum in the middle of the channel's cross section and vanishes on its rigid boundaries. For relatively small values of the Marangoni number, there is no reason for the dependence of the longitudinal velocities on the longitudinal coordinate x. Because of the convective heat transfer, the temperature deviations $\Theta_i(y, z)$ are also maximal in the middle of the channel and decrease towards the rigid boundaries. The inhomogeneity of the temperature in the cross section of the channel generates the

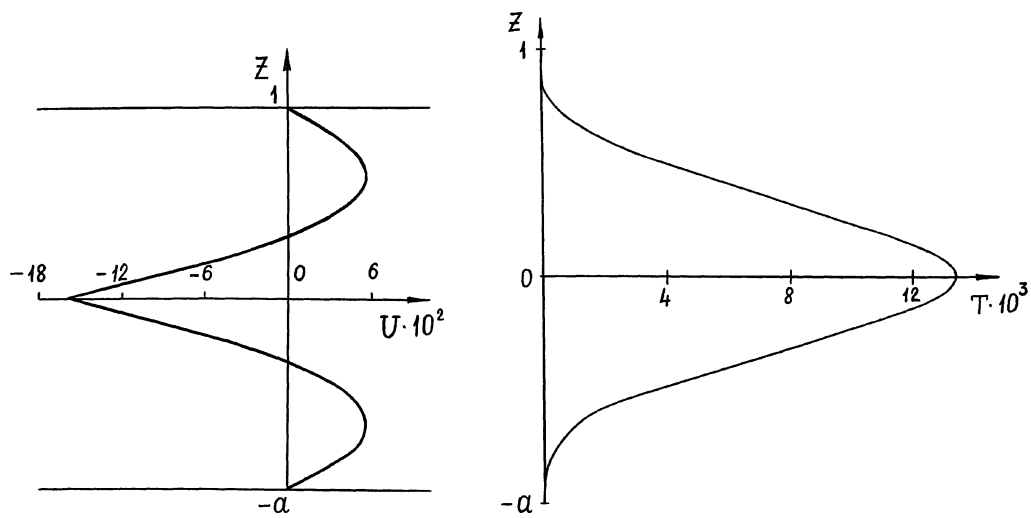

(a) (b)

Figure 2. Profiles of (a) the longitudinal velocity and (b) temperature deviation for the parallel return flow in the model system; $M = 2,\ L = 2.5$.

secondary motion $v_{yi}(y,z)$, $v_{zi}(y,z)$. Thus, one can expect that a 'spiral' flow

$$\mathbf{v}_i = \mathbf{v}_i(y,z), \qquad p_i = p_i(y,z) + B_i x, \qquad T_i = x + \Theta_i(y,z), \quad i = 1,2, \tag{23}$$

will be observed in the system at least for relatively small values of the Marangoni number. In the case of the linear flow, $B_i = 0$. In the case of the return flow, the constants B_i are unknown and should be determined from the conditions (11).

Flows of this kind were first considered by Myznikov [12] for the buoyancy convection in an infinite horizontal layer subject to a horizontal temperature gradient. In that case the spiral flow appeared as a result of the instability of the parallel flow, when the Grashof number exceeded some threshold value. Let us emphasize that in our situation the spiral flow is caused by the lateral boundaries and exists for arbitrarily small values of the Marangoni number. Thus, the appearance of the spiral flow is not related to the instabilities of the parallel flows investigated by Smith and Davis [13].

For spiral flows, the continuity equation

$$\frac{\partial v_{yi}}{\partial y} + \frac{\partial v_{zi}}{\partial z} = 0$$

does not include v_{xi}. That is why it is possible to define the stream functions ψ_i in the following way:

$$v_{yi} = \frac{\partial \psi_i}{\partial z}, \qquad v_{zi} = -\frac{\partial \psi_i}{\partial y}. \tag{24}$$

After elimination of the pressure fields $p_i(y,z)$ in the usual manner, we obtain the following nonlinear boundary value problem:

$$\frac{\partial}{\partial t}\Delta_\perp \psi_i + \frac{\partial \psi_i}{\partial z}\frac{\partial}{\partial y}\Delta_\perp \psi_i - \frac{\partial \psi_i}{\partial y}\frac{\partial}{\partial z}\Delta_\perp \psi_i = c_i \Delta_\perp^2 \psi_i; \tag{25}$$

$$\frac{\partial}{\partial t}U_i + \frac{\partial \psi_i}{\partial z}\frac{\partial}{\partial y}U_i - \frac{\partial \psi_i}{\partial y}\frac{\partial}{\partial z}U_i = c_i \Delta_\perp U_i - e_i B_i; \tag{26}$$

$$\frac{\partial}{\partial t}\Theta_i + \frac{\partial \psi_i}{\partial z}\frac{\partial}{\partial y}\Theta_i - \frac{\partial \psi_i}{\partial y}\frac{\partial}{\partial z}\Theta_i + U_i = \frac{d_i}{P}\Delta_\perp \Theta_i; \tag{27}$$

$$z = 1: \quad \psi_1 = 0, \ \frac{\partial \psi_1}{\partial z} = 0, \ U_1 = 0, \ \Theta_1 = 0; \tag{28}$$

$$z = -a: \quad \psi_2 = 0, \ \frac{\partial \psi_2}{\partial z} = 0, \ U_2 = 0, \ \Theta_2 = 0; \tag{29}$$

$$z = 0: \quad \psi_1 = \psi_2 = 0, \ \frac{\partial \psi_1}{\partial z} = \frac{\partial \psi_2}{\partial z}, \ U_1 = U_2; \tag{30}$$

$$\eta \frac{\partial^2 \psi_1}{\partial z^2} = \frac{\partial^2 \psi_2}{\partial z^2} + \frac{M\eta}{P}\frac{\partial \Theta_1}{\partial y}; \tag{31}$$

$$\eta \frac{\partial U_1}{\partial z} = \frac{\partial U_2}{\partial z} + \frac{M\eta}{P}; \tag{32}$$

$$\Theta_1 = \Theta_2; \tag{33}$$

$$\kappa \frac{\partial \Theta_1}{\partial z} = \frac{\partial \Theta_2}{\partial z}; \tag{34}$$

$$y = \pm L/2: \quad \psi_i = 0,\ \frac{\partial \psi_i}{\partial y} = 0,\ U_i = 0,\ \frac{\partial T_i}{\partial y} = 0, \quad i = 1, 2, \tag{35}$$

where

$$\Delta_\perp = \frac{\partial^2}{\partial y^2} + \frac{\partial^2}{\partial z^2}, \qquad U_i = v_{xi}, \qquad c_1 = d_1 = e_1 = 1, \qquad c_2 = 1/\nu, \qquad d_2 = 1/\chi, \qquad e_2 = \rho.$$

In the case of the linear flow,

$$B_1 = B_2 = 0. \tag{36}$$

In the case of the return flow, the constants $B_i,\ i = 1, 2$, should be found from the conditions

$$\int_{-L/2}^{L/2} dy \int_0^1 dz\, U_1 = 0, \qquad \int_{-L/2}^{L/2} dy \int_{-a}^0 dz\, U_2 = 0. \tag{37}$$

For the calculation of B_i and the fields U_i that satisfy the conditions (37), the following procedure is applied. The functions U_i are presented in the form

$$U_i = \widetilde{U}_i + \sum_{j=1}^{2} e_j B_j V_{ij}, \quad i = 1, 2,\ j = 1, 2, \tag{38}$$

where $\widetilde{U}_i$ and V_{ij} satisfy the following equations and boundary conditions:

$$\frac{\partial}{\partial t}\widetilde{U}_i + \frac{\partial \psi_i}{\partial z}\frac{\partial}{\partial y}\widetilde{U}_i - \frac{\partial \psi_i}{\partial y}\frac{\partial}{\partial z}\widetilde{U}_i = c_i \Delta_\perp U_i; \tag{39}$$

$$z = 1: \quad \widetilde{U}_1 = 0; \qquad z = -a: \quad \widetilde{U}_2 = 0; \tag{40}$$

$$z = 0: \quad \widetilde{U}_1 = \widetilde{U}_2,\ \eta \frac{\partial \widetilde{U}_1}{\partial z} = \frac{\partial \widetilde{U}_2}{\partial z} + \frac{M\eta}{P}; \tag{41}$$

$$y = \pm L/2: \quad \widetilde{U}_i = 0; \tag{42}$$

$$\frac{\partial}{\partial t}V_{ij} + \frac{\partial \psi_i}{\partial z}\frac{\partial}{\partial y}V_{ij} - \frac{\partial \psi_i}{\partial y}\frac{\partial}{\partial z}V_{ij} = c_i \Delta_\perp V_{ij} - \delta_{ij}; \tag{43}$$

$$z = 1: \quad V_{1j} = 0; \qquad z = -a: \quad V_{2j} = 0; \tag{44}$$

$$z = 0: \quad V_{1j} = V_{2j},\ \eta \frac{\partial V_{1j}}{\partial z} = \frac{\partial V_{2j}}{\partial z}; \tag{45}$$

$$y = \pm L/2: \quad V_{ij} = 0; \tag{46}$$

$i = 1, 2$, $j = 1, 2$; δ_{ij} is the Kronecker symbol. After calculation of $\widetilde{U}_i$ and V_{ij}, the expression (38) is substituted into the conditions (37), and the system of two linear algebraic equations for B_j is solved.

The boundary value problem (25)–(35) is solved by the finite difference method. The variables "stream function – vorticity" are used to solve Eq. (25) with corresponding boundary conditions (for details, see Simanovskii and Nepomnyashchy [8]). Equations (25)–(35) are approximated on a uniform mesh using a second order approximation for the spatial coordinates. The integration of the evolution equations is performed by means of an explicit scheme. The advantage of this method of approximation is the simplicity of the formulas. However, when using this approach one should be careful with the choice of the mesh size and the time step. From the point of view of the approximation of spatial derivatives, the most dangerous region is the region around the "cold corners" where the interface comes into contact with the lateral rigid walls (see Canright [14]). Using the estimates given by Canright [14], we chose the mesh size smaller than the minimal characteristic scale of the flow near the corner. The rectangular 42×56 and 84×56 meshes were used according to the Marangoni number. To estimate the reliability of the results obtained, we performed control calculations with a mesh 128×56. The time step was chosen from the solvability condition.

To test the numerical code, we calculated numerically the profiles of the longitudinal velocities U_i and temperature deviations Θ_i, $i = 1, 2$, corresponding to the exact solutions (12)–(15) and (17)–(20) (on the lateral boundaries $y = \pm L/2$ we used the boundary conditions $\partial v_{xi}/\partial y = \partial v_{zi}/\partial y = v_{yi} = 0$ instead of the boundary conditions $\mathbf{v}_i = 0$). An example of the profiles calculated for the model system with the following set of parameters: $\eta = \nu = 0.5$, $\kappa = \chi = 1$, $P = 1$, $a = 1$ is shown in *figure 2*. For this example, the relative error was less than 0.4% for the velocity profile and less than 4% for the temperature profile. Also, we calculated the threshold of the oscillatory instability of the parallel flows (12)–(15) and (17)–(20) with respect to the transverse hydrothermal waves (*a*) by means of our numerical code with the above-mentioned boundary conditions and (*b*) by solving the linearized eigenvalue problem using the Runge–Kutta method. The calculated threshold Marangoni numbers were compared. The relative error was less than 6%. The results could not be directly compared with those of Smith and Davis [13] because of the different thermal boundary conditions on the horizontal rigid boundaries.

The boundary value problem (25)–(37) contains eight independent nondimensional parameters, and the parametric investigation of this problem is thus extremely cumbersome. We shall focus on some particular fluid systems.

3. Numerical results

3.1. Steady motions

First, let us consider the linear flow in the above-mentioned model system.

As was explained in Section 2, for arbitrarily small values of the Marangoni number, the longitudinal temperature gradient generates a non-zero field of longitudinal velocity $U_i(y, z)$. In the case of linear flow, $U_i(y, z) \leqslant 0$. The field $|U_i(y, z)|$ has a maximum in the middle of the channel and vanishes on its rigid boundaries due to the viscous friction (see *figure 3(a)*). One can see from *figure 3(c)* that the temperature deviations $\Theta_i(y, z) \geqslant 0$ (see discussion in Section 2). They are maximal in the middle of the channel and decrease towards the rigid boundaries. The inhomogeneity of the temperature in the cross section of the channel generates a secondary motion $\psi_i(y, z)$ which has a four-vortex structure (see *figure 3(b)*). The spiral thermocapillary motion satisfies the following symmetry conditions:

$$\psi_i(y, z) = -\psi_i(-y, z), \qquad U_i(y, z) = U_i(-y, z), \qquad \Theta_i(y, z) = \Theta_i(-y, z). \tag{47}$$

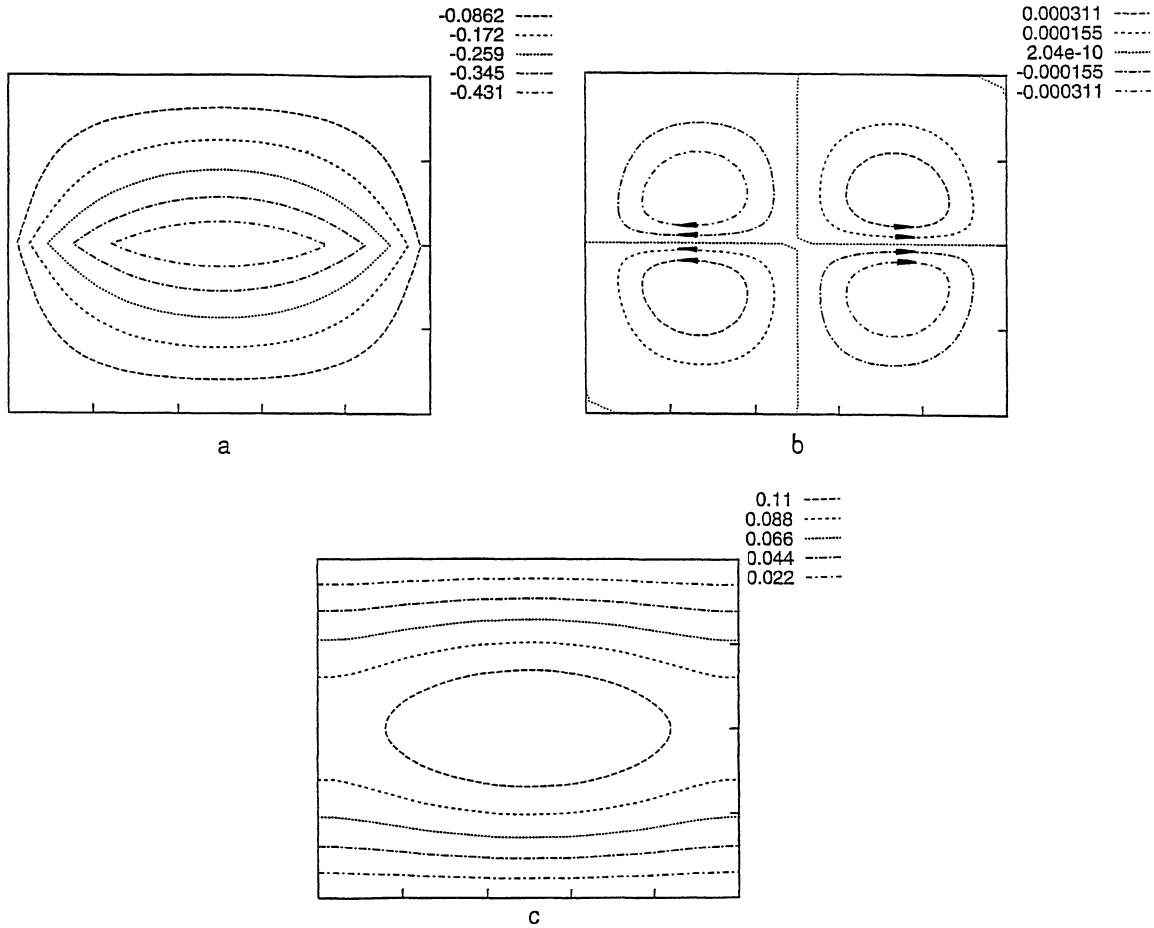

Figure 3. Isolines of the longitudinal velocity (a), stream function (b) and temperature deviation (c) for a steady thermocapillary motion in the model system; $M = 2,\ L = 2.5$ (linear flow).

The motion symmetry is sustained for relatively large Marangoni numbers, but the shape of the vortices is changed (see *figure 4(a)*). The maximum of intensity of the transverse flow is displaced to the corner points of the interface. This displacement is especially obvious in the case of larger values of the width parameter L (see *figure 5(a)*): the transverse flow is located near the lateral boundaries of the channel.

The physical nature of the observed phenomenon is as follows: the flow along the interface towards the relatively cold wall compresses the thermal gradient, thereby enhancing the flow. This phenomenon was studied earlier for two-dimensional flows by Zebib et al. [15] and Canright [14], and for axisymmetric flows by Shevtsova et al. [16].

Motions of a similar structure were found for the real air-water system with the parameters $\eta = 0.0182,\ \nu = 15.1,\ \kappa = 0.0396,\ \chi = 138,\ P = 0.758$ (see *figure 4(b), L* $= 2.5$; *figure 5(b), L* $= 6.8$).

Now we shall consider spiral motions in a closed cavity (return flow). First, let us discuss the case of the model system. In the return flow, the longitudinal velocity $U_i(y, z)$ is negative near the interface (i.e. the fluids flow from the hot end of the cavity to the cold one) and positive near the horizontal rigid boundaries (i.e. the fluids flow from the cold end of the cavity to the hot one; see *figure 6(a)*). That is why the fields of the temperature deviations $\Theta_i(y, z)$ in the cases of a return flow (*figure 6(c)*) and a linear flow (*figure 3(c)*) differ

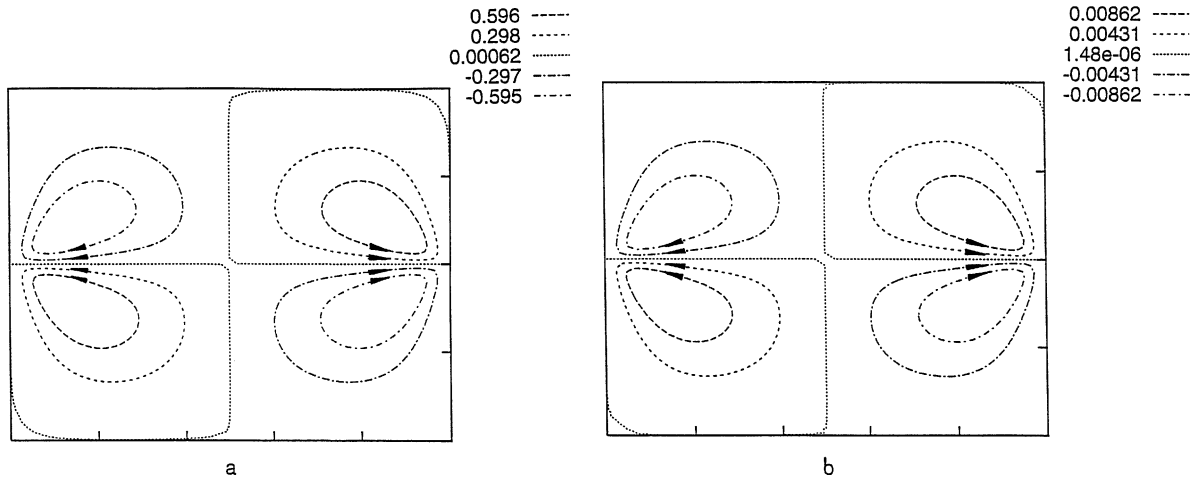

Figure 4. Stream lines (a) for the model system; $M = 660,\ L = 2.5$; (b) for the air-water system; $M = 146,\ L = 2.5$ (linear flow).

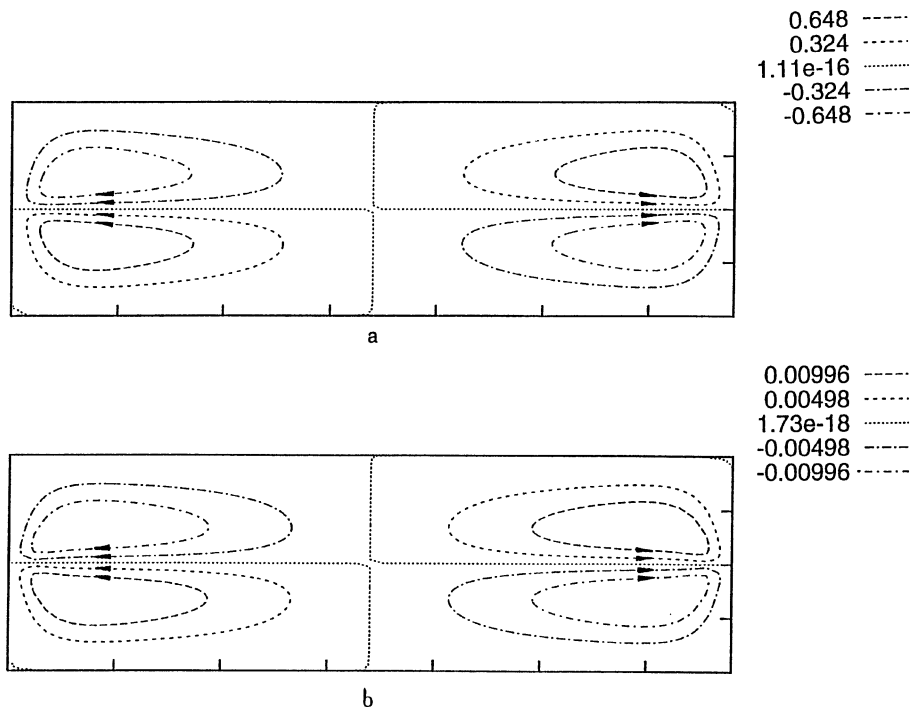

Figure 5. Stream lines (a) for the model system; $M = 200,\ L = 6.8$; (b) for the air-water system; $M = 83.3,\ L = 6.8$ (linear flow).

considerably. For the return flow, two relatively cold zones are generated near the horizontal rigid boundaries. Nevertheless, at the interface the temperature deviations $\Theta_i(y, z)$ are maximal in the middle of the cavity and decrease towards the rigid boundaries (see *figure 6(c)*). Therefore, the generated secondary four-vortex motion $\psi_i(y, z)$ has the same direction of rotation as in the case of the linear flow (see *figure 6(b)*). The spiral thermocapillary motion satisfies the symmetry conditions (47).

Motions of a similar structure were also found for the considered air-water system (see *figure 7*).

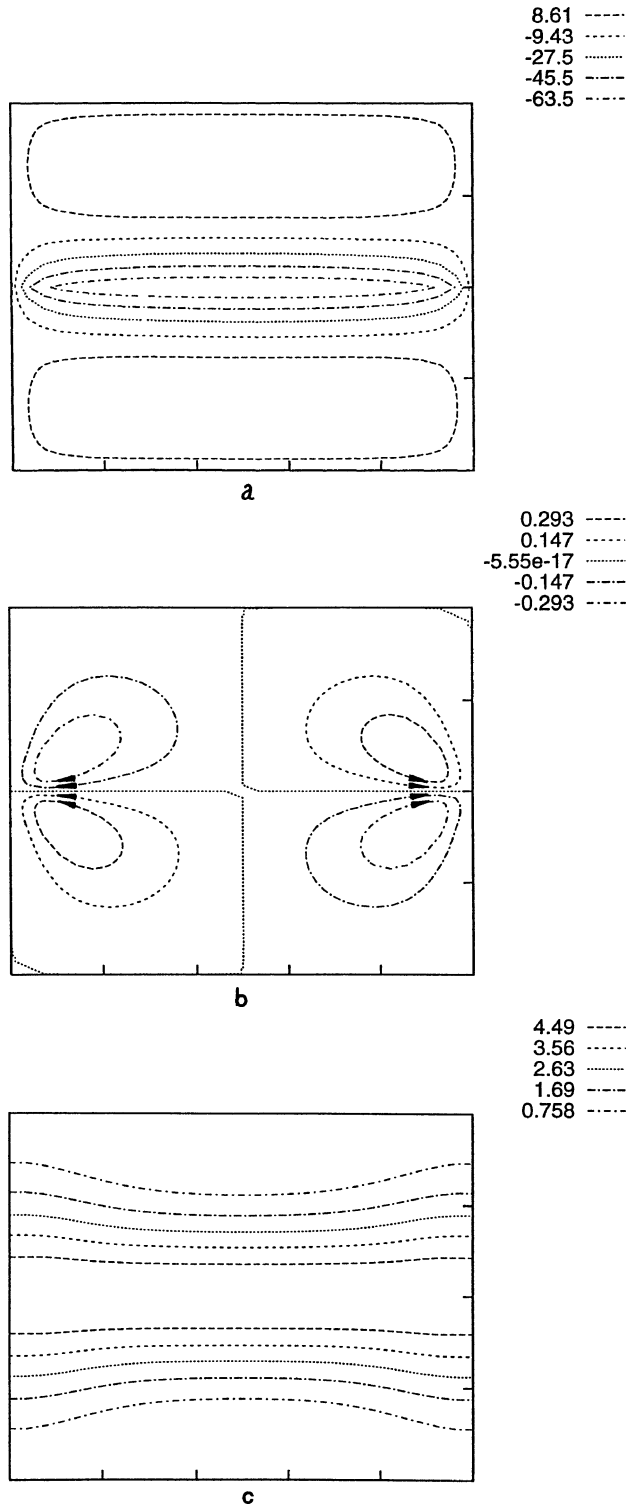

Figure 6. Isolines of (a) the longitudinal velocity; (b) stream function and (c) temperature deviation for a steady thermocapillary motion in the model system; $M = 1000$ (return flow).

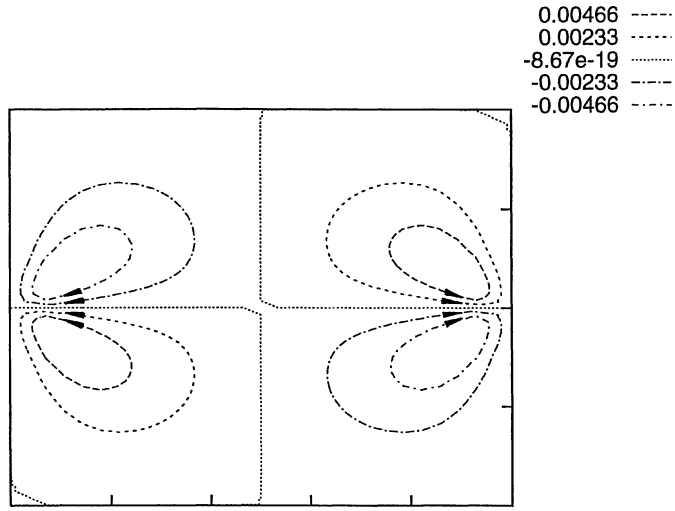

Figure 7. Stream lines for a steady thermocapillary motion in the air-water system; $M = 333.2$ (return flow).

3.2. Oscillatory motions

The numerical simulation of the system (25)–(37) shows that when the Marangoni number exceeds some threshold value, the steady motion is replaced by the time-periodic oscillatory regime. This means that the steady spiral motion caused by the influence of rigid lateral boundaries becomes oscillatorily unstable.

In order to investigate the stability of the stationary motion (23), it is necessary to linearize the boundary value problem (1)–(11) around the solution (23). The normal disturbances of the flow (23) have the structure $f(y,z;k)\exp(ikx+\lambda t)$ where $f(y,z;k) = (\tilde{\mathbf{v}}_i(y,z), \tilde{p}_i(y,z), \widetilde{\Theta}_i(y,z))$, k is the longitudinal wavenumber, $\mathrm{Re}\,\lambda$ is the growth rate and $\mathrm{Im}\,\lambda$ is the frequency of the disturbance. One obtains the eigenvalue problem which determines an infinite number of normal modes $f^{(n)}(y,z;k)$, $n = 1, 2, \ldots$, and the dependence $\lambda = \lambda^{(n)}(k)$ for each normal mode.

Let us discuss some general features of the spectrum of normal modes.

As the original equations are real, we come to the following conclusion: if $f^{(n)}(y,z;k)$ is a solution of the eigenvalue problem with the wavenumber k and the eigenvalue $\lambda^{(n)}(k)$, then $f^{(n)*}(y,z;k)$ is a solution of the eigenvalue problem with the wavenumber $-k$ and the eigenvalue $\lambda^{(n)*}(k)$, where $*$ means complex conjugate. There are two possibilities (Nepomnyashchy [17]):

(I) either eigenfunction belongs to the same mode:

$$f^{(n)*}(y,z;k) = f^{(n)}(y,z;-k), \qquad \lambda^{(n)*}(k) = \lambda^{(n)}(-k); \tag{48}$$

(II) the eigenfunctions belong to different modes:

$$f^{(n)*}(y,z;k) = f^{(m)}(y,z;-k), \qquad \lambda^{(n)*}(k) = \lambda^{(m)}(-k), \quad m \neq n. \tag{49}$$

In the former case, the growth rate $\mathrm{Re}\,\lambda^{(n)}(k)$ is an even function of k, while the frequency $\mathrm{Im}\,\lambda^{(n)}(k)$ is an odd function of k. The eigenvalue $\lambda^{(n)}(0)$ is real. If the corresponding mode generates an instability, the condition $\mathrm{Re}\,\lambda^{(n)}(k, M_*) = 0$ determines the neutral stability curve $M = M_*(k)$. Obviously, $dM_*/dk = 0$ as $k = 0$. Depending on the sign of d^2M_*/dk^2, the point $k = 0$ corresponds to a minimum or a maximum of $M(k)$.

In the latter case, the growth rate and the frequency are neither even nor odd functions of k. Both $\lambda^{(n)}(0)$ and $\lambda^{(m)}(0) = \lambda^{(n)*}(0)$ are eigenvalues. In the case of instability, there are *two* neutral curves $M = M_+(k)$ and $M = M_-(k)$ which are determined by the conditions $\mathrm{Re}(\lambda^{(n)}(k, M_+)) = 0$ and $\mathrm{Re}(\lambda^{(m)}(k, M_-)) = 0$ respectively. One can see that $M_+(k) = M_-(-k)$, so that $M_+(0) = M_-(0)$. Generally (i.e. except manifolds of the codimension 1 in the parameter space) $dM_+/dk = -dM_-/dk \neq 0$ as $k = 0$. Thus, the minimum of the neutral curve is located at $k \neq 0$ in this case.

Using the system (25)–(37), one can investigate the stability of the stationary flow (23) only with respect to the disturbances which do not depend on the longitudinal coordinate x, i.e. with $k = 0$. In the case (I) one obtains a 'monotonic' instability at $k = 0$, which should generate a new stationary spiral flow. If the neutral curve $M_*(k)$ has a minimum at $k = 0$, one can expect this flow to be stable near the bifurcation point. In the case (II) the instability is 'oscillatory' at $k = 0$, and it leads to the appearance of time-periodic spiral motions. In the latter case, however, the point $k = 0$ does not generally correspond to the minimum of the neutral curve, so that one can expect that near the bifurcation point the spiral flow will not be stable with respect to the x-dependent disturbances.

The complete analysis of the stability problem for arbitrary k is beyond the scope of the present paper which is based on the boundary value problem (25)–(35). But even the calculation of the eigenvalues $\lambda^{(n)}(0)$ alone is not a simple task. The main problem is the behavior of the vorticity field near the corner points where the interface comes into contact with the lateral rigid walls. The vorticity field depends on the polar angle and is not continuous in the corner points (Moffat [18]). This circumstance makes it difficult to use methods based on the approximation of fields by series of smooth functions. For this reason the instability threshold was determined in the following way. We simulated the evolution of small disturbances of a steady spiral flow by means of the numerical algorithm described above. The analysis of small-amplitude oscillations enabled us to calculate the growth (or decay) rate and the frequency of the disturbance for the mode generating the instability.

Our simulations performed for the model and the air-water systems revealed an instability of type (II). For instance, in the case of the air-water system in a cavity with $L = 2.5$, the critical Marangoni number with respect to the disturbances with $k = 0$ is around $M = 380$, and the critical frequency is approximately $\omega = 3.3$. As was explained above, the most dangerous disturbances in this case correspond to the longitudinal wavenumber $k \neq 0$. From the physical point of view, two relevant modes of disturbances (with positive and negative frequency values) correspond to the waves propagating in opposite directions. Since the mean longitudinal flow is asymmetric with respect to the transformation $x \to -x$, the interaction of the disturbances with this flow depends on the direction of the wave's motion. As a result, this interaction supports a definite kind of wave, and hence 'wavy' flows with $k \neq 0$, rather than 'oscillatory' spiral motions with $k = 0$, are likely to be observed in the experiment. However, we can expect that in some cases the main physical mechanism of the instability itself does not depend on the direction of the waves' propagation and can be understood by the investigation of the spiral motions. There is a need therefore to describe such motions obtained by the direct numerical simulation of the system (25)–(37).

To characterize the intensity and the symmetry properties of the flows, we introduce the following integral characteristics:

$$S_{1l}(t) = \int_{-L/2}^{0} dy \int_0^1 dz\, \psi_1(y, z, t), \qquad S_{1r}(t) = \int_0^{L/2} dy \int_0^1 dz\, \psi_1(y, z, t); \tag{50}$$

$$S_{2l}(t) = \int_{-L/2}^{0} dy \int_{-a}^{0} dz\, \psi_2(y, z, t), \qquad S_{2r}(t) = \int_0^{L/2} dy \int_{-a}^{0} dz\, \psi_2(y, z, t). \tag{51}$$

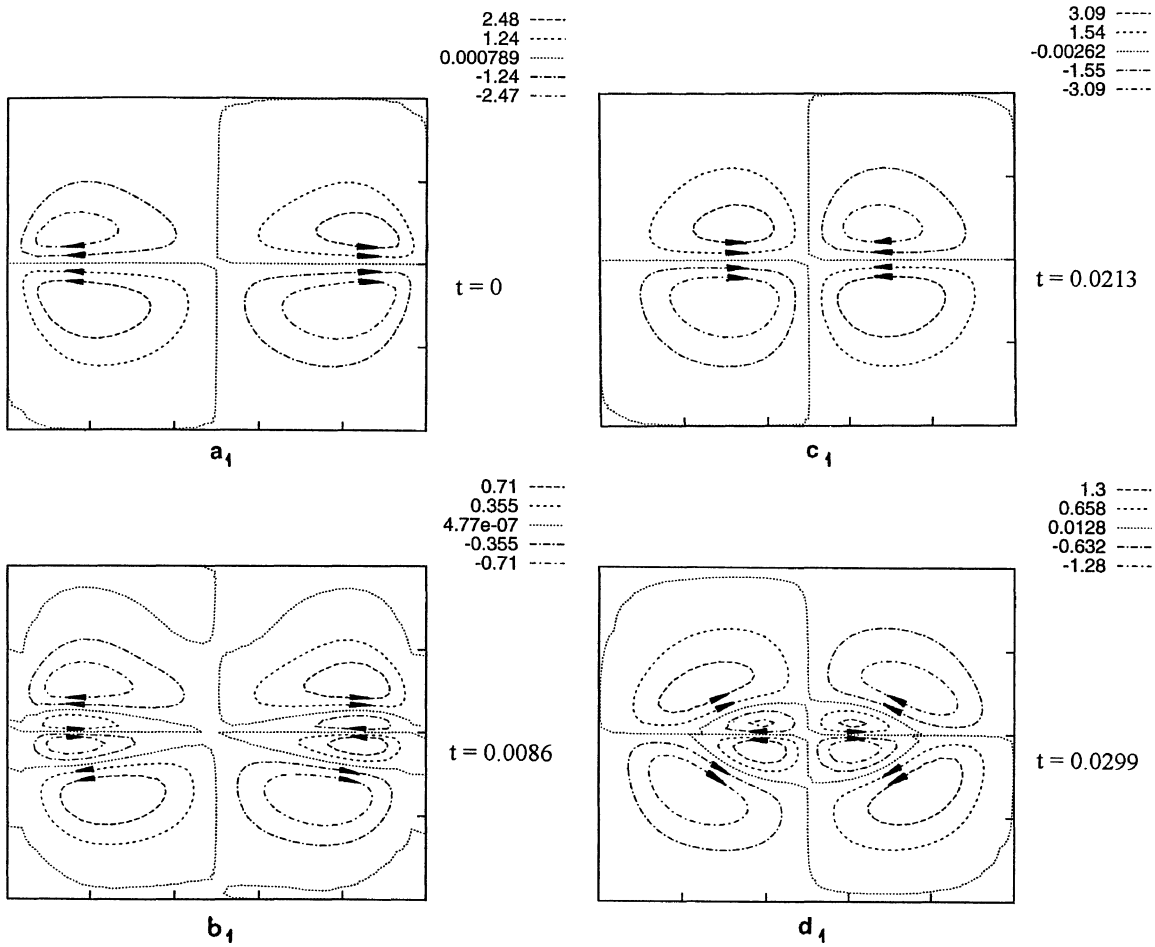

Figure 8. Stream lines (a_1)–(d_1) and temperature deviation isolines (a_2)–(d_2) for the model system; $M = 1700$.

For model and real systems, for both linear and return flows we found two different types of the oscillatory motions. To illustrate the characteristic features of oscillations, it is more convenient to consider the case of the return flow in the model system.

The first type is characterized by the symmetry property (47). For this type of motion, $S_{ir}(t) = -S_{il}(t),\ i = 1, 2$.

Let us describe the evolution of the stream function and the temperature fields during one period (the changes in the field of the longitudinal velocity are relatively small). The intensive secondary motion (*figure 8(a_1)*) leads to the temperature growth at the interface near the lateral walls (*figures 8(a_2), 8(b_2)*). As a result, the direction of the transverse horizontal temperature gradient changes, and four new vortices appear near the interface (*figure 8(b_1)*). The direction of the new vortices' rotation is opposite to that of the old ones. The new vortices grow and suppress the old vortices. A new four-vortex structure is established in the system (*figure 8(c_1)*). Comparing *figure 8(a_1)* and *figure 8(c_1)*, one can see that the direction of rotation changes during a half-period. Note that the shape and the intensity of the vortices shown in *figure 8(a_1)* and *8(c_1)* are not identical. The temperature in the middle of the channel grows, the horizontal temperature gradient is now directed from the middle to the lateral boundaries of the channel *figure 8(c_2)*, and again four new vortices appear near the interface

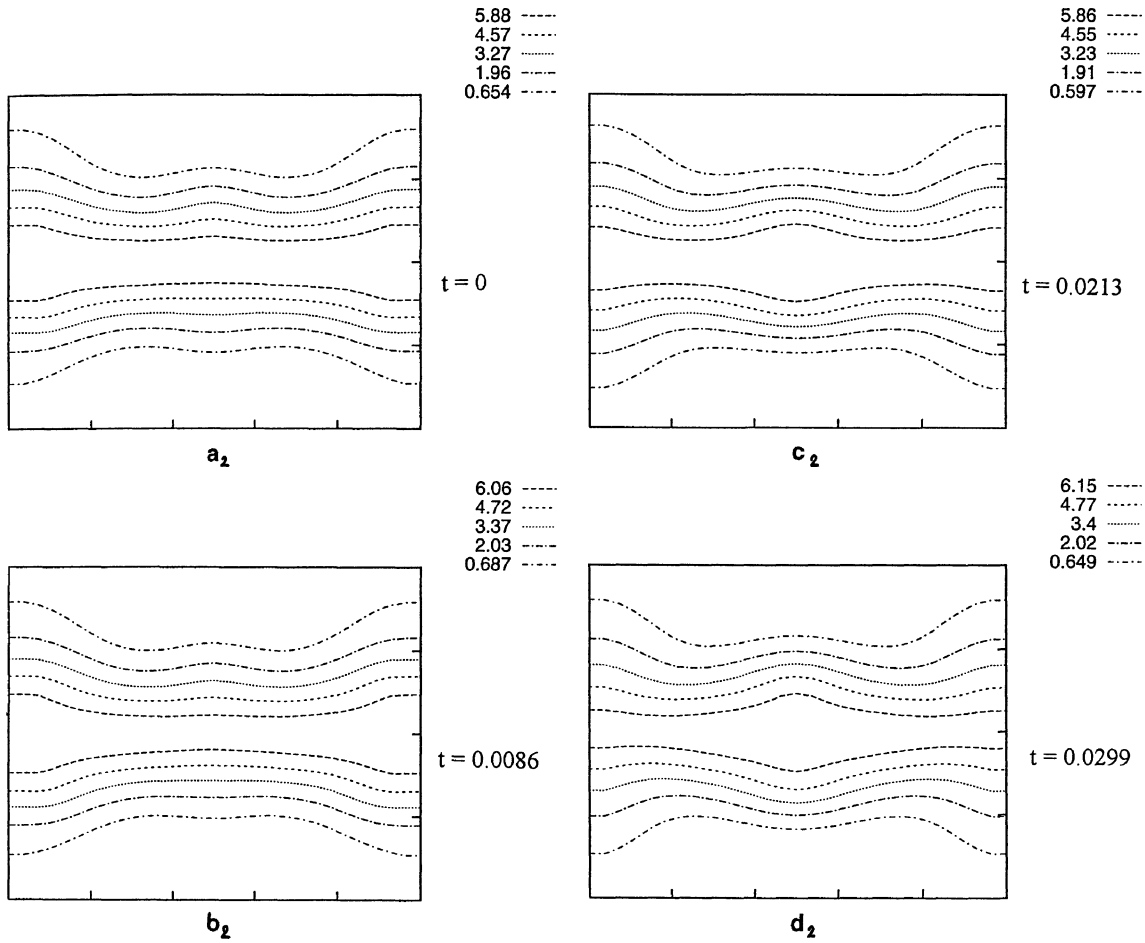

Figure 8. (Continued).

(*figure 8(d$_1$)*). The new vortices grow and replace the old ones, and this concludes one oscillation period (*figure 8(a$_1$)*). The period of oscillations decreases with the growth of the Marangoni number (see *figure 9*, line 1). The stability region for this type of oscillations is relatively small: $1500 < M < 1700$.

For smaller and larger values of the Marangoni number one observes the transition to the second type of oscillations. For the second type of oscillations the symmetry property (47) is violated, and another set of symmetry relations,

$$\psi_i(y, z, t + \tau/2) = -\psi_i(-y, z, t), \qquad U_i(y, z, t + \tau/2) = U_i(-y, z, t), \tag{52}$$

hold. The number of vortices in each layer changes during the period of oscillations. The dependence of the oscillation period for this type of motion is shown in *figure 9* (line 2). A typical evolution of the stream line patterns is shown in *figure 10*. The physical mechanism of the oscillations is essentially the same as in the case of the symmetric oscillations, but the spatial structure of the flow is different. A new pair of vortices is always generated near the lateral boundaries. The asymmetric oscillations are observed in a rather large region of the Marangoni number: $1250 < M < 2500$. We did not perform calculations for $M > 2500$. A typical phase trajectory in the plane (S_{1l}, S_{1r}) for this type of motion is shown in *figure 11*.

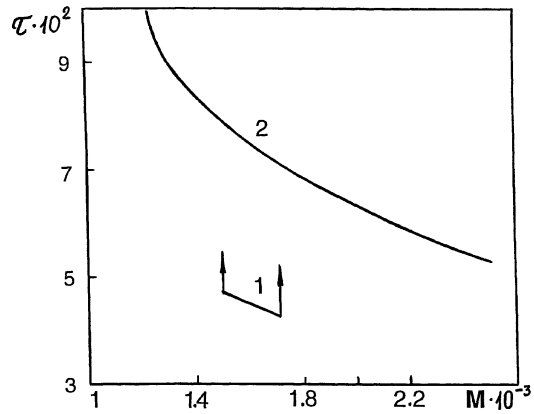

Figure 9. Dependence of the period on the Marangoni number for symmetric (line 1) and asymmetric (line 2) oscillations; model system.

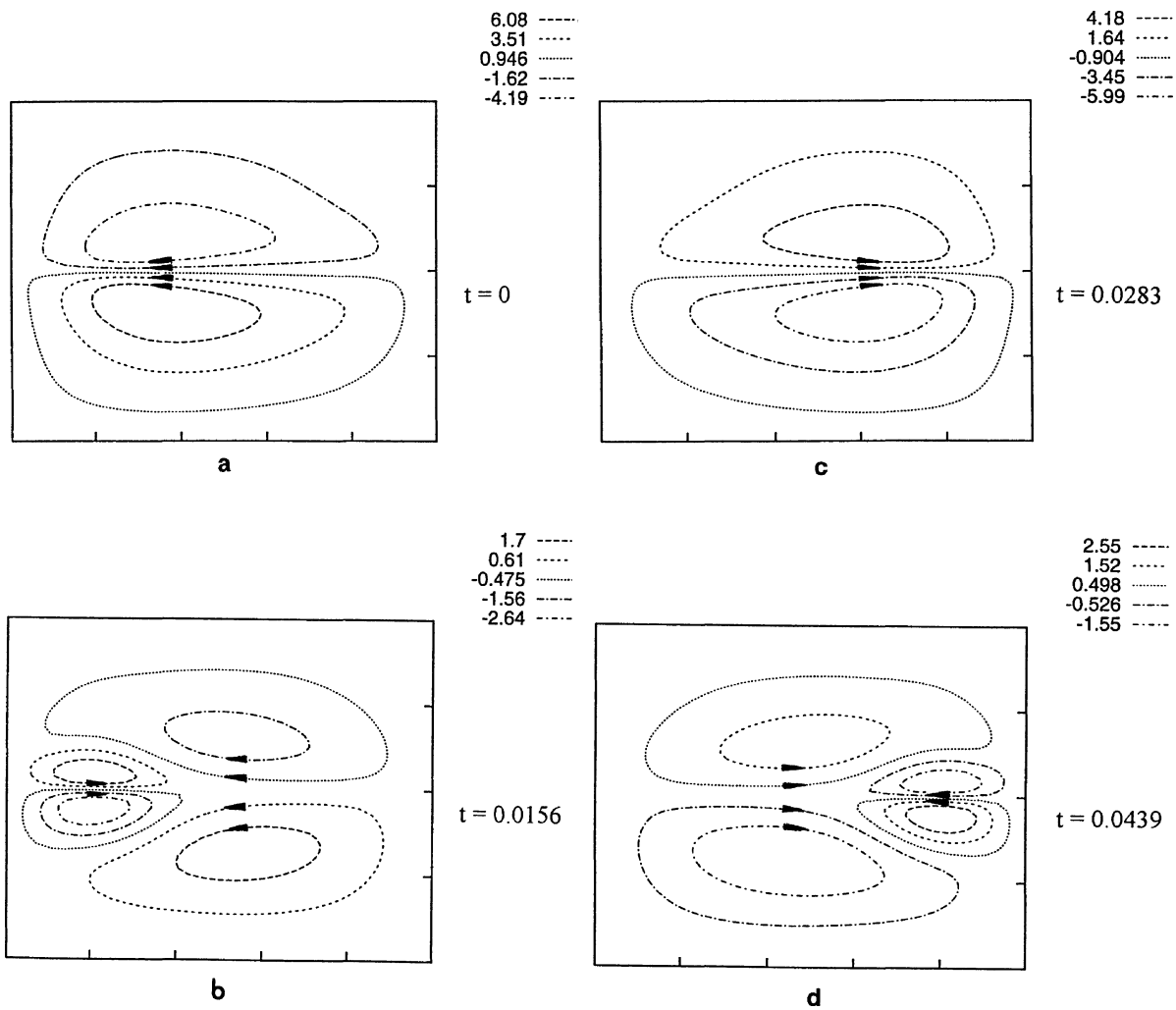

Figure 10. Evolution of stream lines for the asymmetric oscillations in the model system; $M = 2300$.

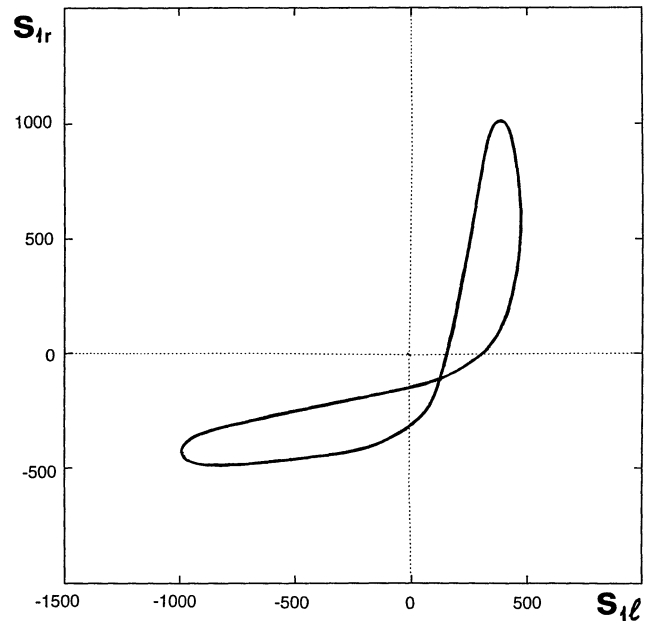

Figure 11. Phase trajectory in the plane (S_{1l}, S_{1r}) for the asymmetric oscillations in the model system; $M = 2300$.

We found the same two oscillatory regimes in the air-water system. However, the symmetric type (47) of oscillations is stable in a relatively larger interval of Marangoni number ($400 \leqslant M \leqslant 490$). The mechanism of the oscillatory motion in the water layer is essentially the same as in the model system, but new vortex pairs which replace the vortices of the previous generation occur in the middle of the channel. A similar process takes place in the air layer as well, but the flow structure in the air is much less inertial and is mainly determined by the temperature and flow fields in the water near the interface. The evolution of the stream lines is shown in *figure 12*. The asymmetric type of oscillations (52) is found in the region $M \geqslant 500$. In the water layer, the flow pattern can be considered as a non-stationary superposition of a two-vortex structure and a one-vortex structure. The flow in the air layer develops faster than that in the water and is mainly determined by the temperature and flow fields in the water (see *figure 13*). The orbits in the phase space for the asymmetric oscillations are shown in *figure 14*.

Similar oscillations were obtained in the case of the basic linear flow.

4. Discussion of results and concluding remarks

The numerical simulations described here revealed the existence of two qualitatively different regimes of thermocapillary flows in a channel.

For relatively small values of the Marangoni numbers, a steady three-dimensional flow is observed, which is a superposition of a one-dimensional flow along the channel and a two-dimensional four-vortex flow in the cross section of the channel. As was explained above, the transverse motion is caused by the existence of the vertical lateral rigid boundaries.

Another kind of flow occurs for larger values of the Marangoni number. In the framework of the applied approach, we found the threshold of the occurrence of 'homogeneous oscillations' but not 'waves' generation. In the case of a channel with the relative width $L = 2.5$ that contained a layer of air and a layer of water

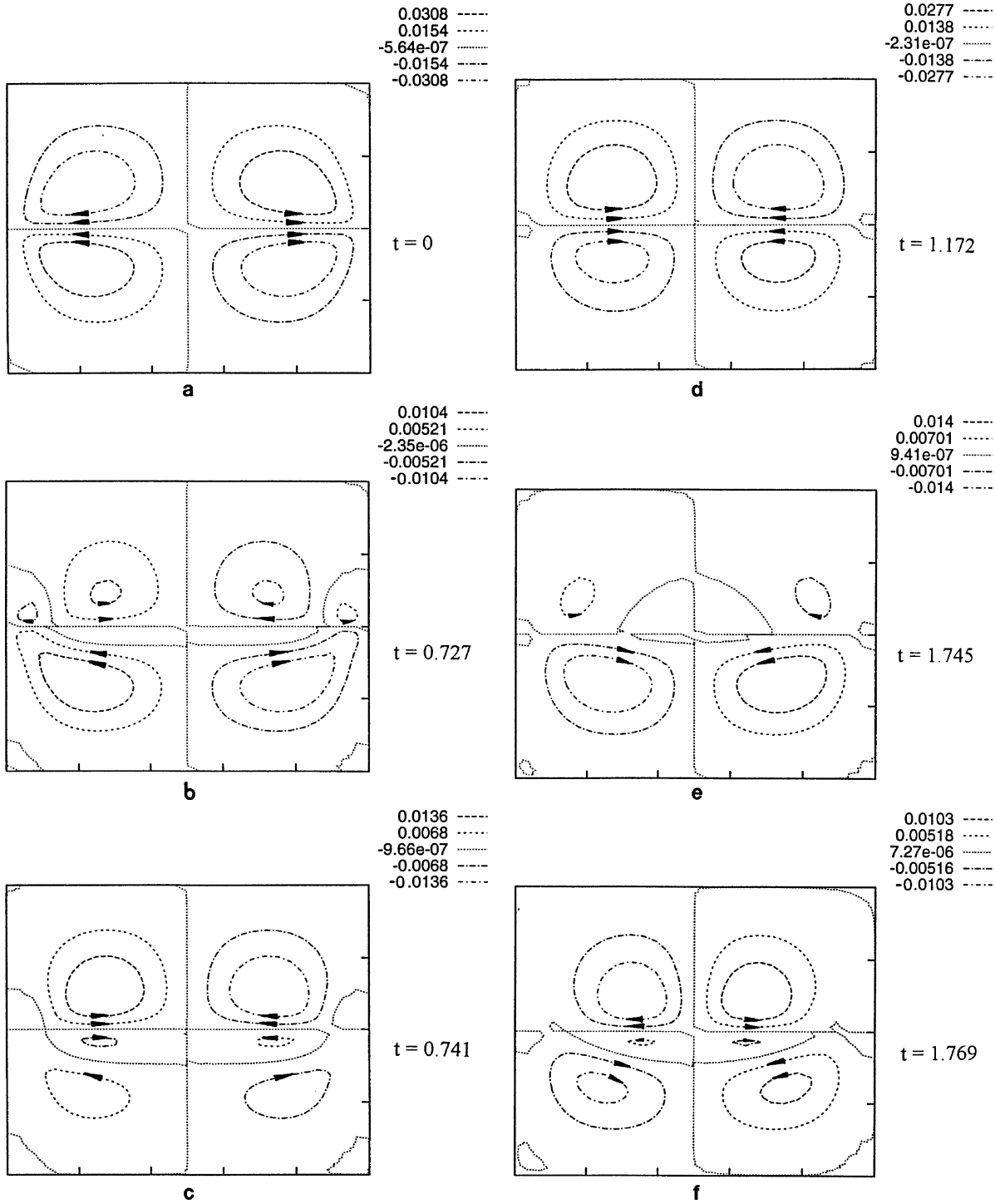

Figure 12. Stream lines for the air-water system; $M = 396$.

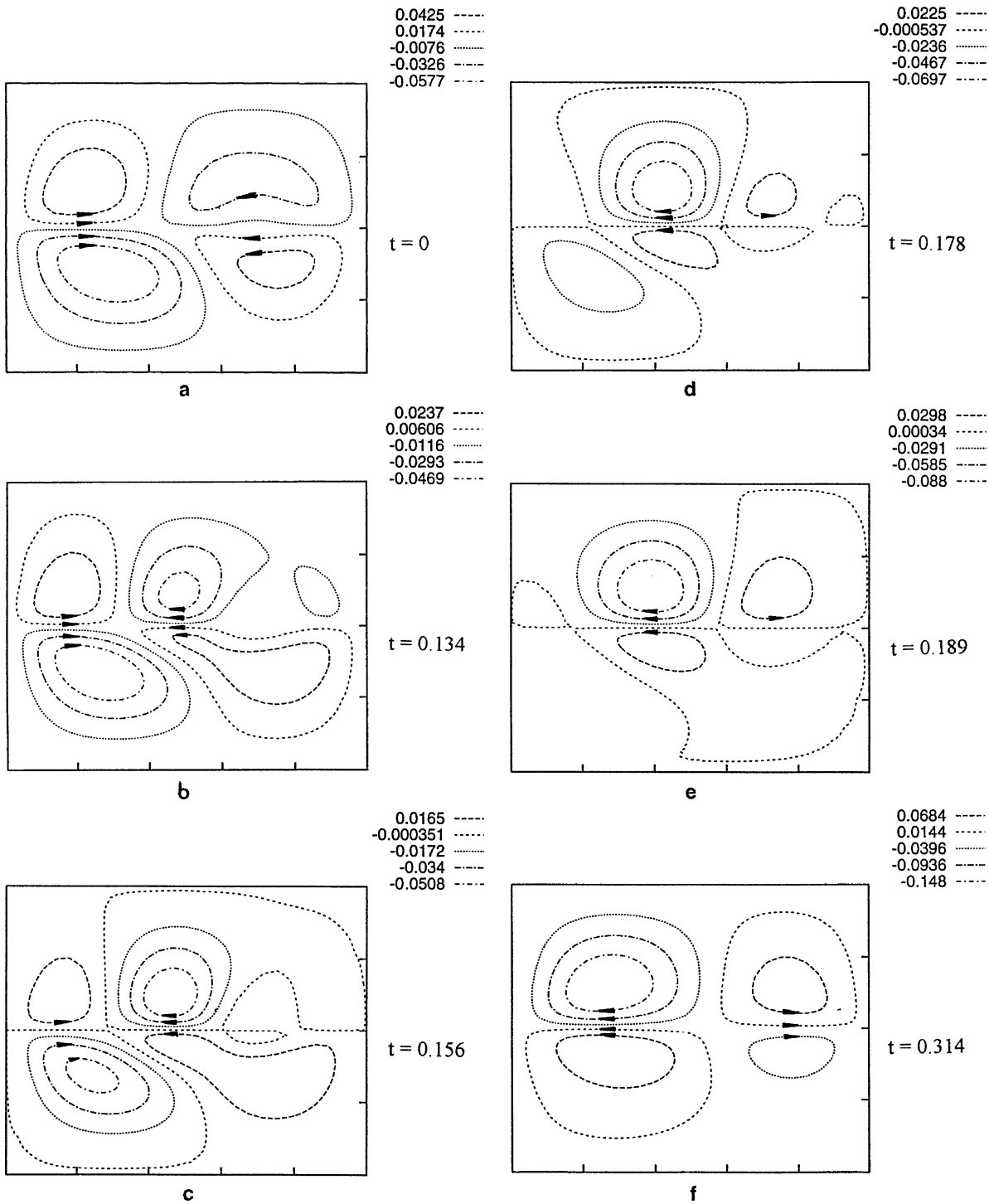

Figure 13. Stream lines for the asymmetric oscillations in the air-water system during one half of the period; $M = 500$.

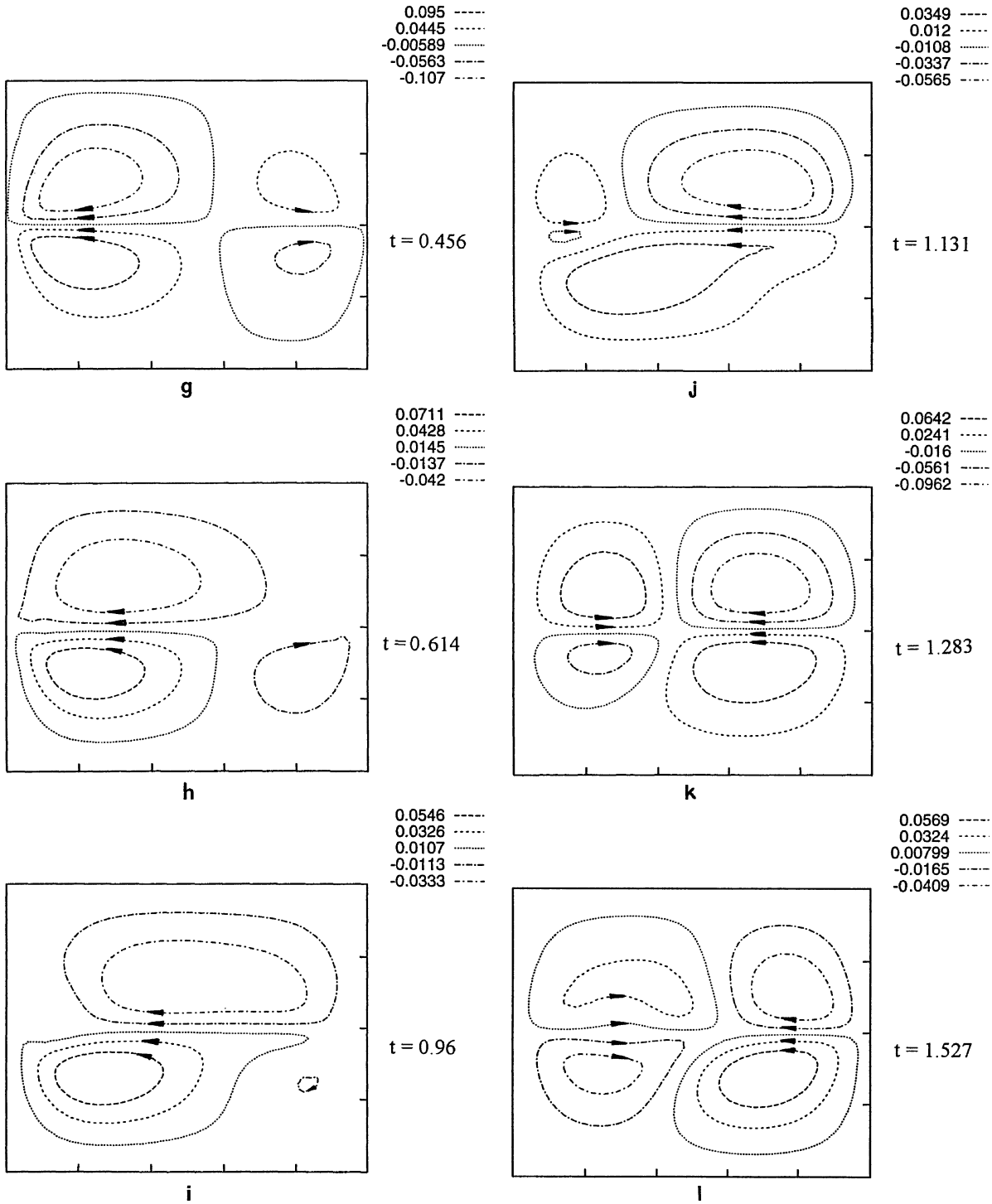

Figure 13. (Continued).

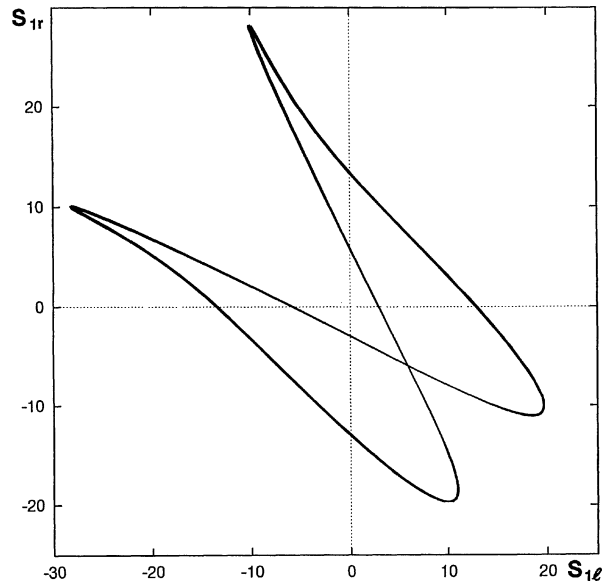

(a)

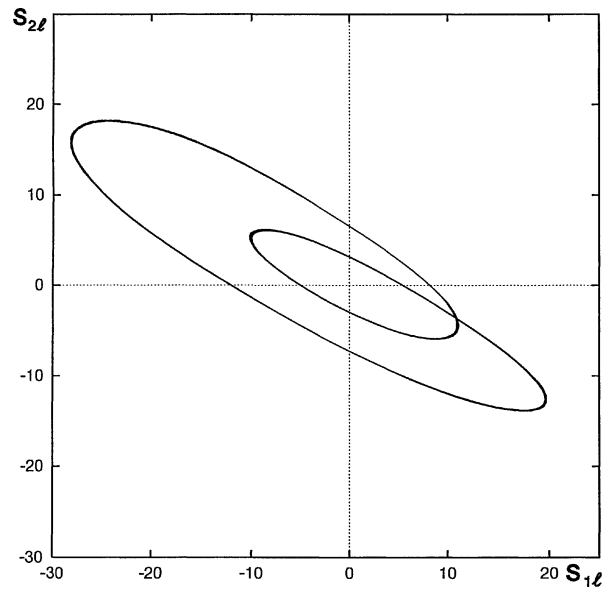

(b)

Figure 14. Phase trajectories (a) in the plane (S_{1l}, S_{1r}) and (b) in the plane (S_{1l}, S_{2l}) for the asymmetric oscillations in the air-water system; $M = 500$.

with equal thicknesses ($a = 1$), the instability threshold for oscillations is found to be equal to $M = 380$. For example, if the full thickness of the channel is $2a_1 = 1$ cm, the oscillations will occur for the temperature gradient A larger than 0.35 K/cm.

As to the physical nature of the instability observed in our simulations, we can suggest that these oscillations are a manifestation of the 'hydrothermal waves' discovered by Davis [3] in the case of parallel flows. Because of

the geometry of the considered problem, one observes a 'standing' hydrothermal wave that comes to replace the steady spiral flow. The influence of the lateral boundary conditions on this kind of flow is of minor importance: the rigid boundary conditions increase the critical Marangoni number.

To justify this conjecture, we performed simulations with periodic boundary conditions on the lateral boundaries which correspond to a laterally infinite two-layer system. In this case, for relatively small values of the Marangoni number, the parallel flow is observed instead of the steady spiral flow. As the Marangoni number grows, the parallel flow becomes unstable with respect to the hydrothermal waves. The linear instability threshold can be easily calculated, and it is equal to $M = 180$ for the air-water system; the critical wavenumber is $k = 2.1$. The nonlinear numerical simulations performed in the region with $L = 2.75$ ($k = 2\pi/L = 2.28$) showed that the oscillations occurred at $M \approx 210$, which is in a reasonable agreement with the predictions of the linear theory. The shape of the oscillations is very similar to that of symmetric oscillations in the channel with rigid boundaries.

We expect that both regimes of the oscillatory spiral flows found in our simulations are unstable with respect to three-dimensional disturbances which lead to non-synchronous oscillations in different cross-sections of the channel. The investigation of the latter effect can be done only by complete three-dimensional simulations.

Acknowledgements

This work was supported in part by the German-Israeli Foundation for Scientific Research and Development and by E. and J. Bishop Research Fund. I.B.S. acknowledges the support of the Israeli Ministry of Science and Humanities and the Israeli Ministry for Immigrant Absorption. I.B.S. also is grateful to D. Kessler for his valuable advice and to L. Shtilman for his encouragement.

References

[1] Levich V.G., Physicochemical Hydrodynamics, Prentice-Hall, Englewood Cliffs, NJ, 1962.
[2] Birikh R.V., Thermocapillary convection in a horizontal layer of liquid, J. Appl. Mech. Tech. Phys. 7 (1966) 43–49.
[3] Davis S.H., Thermocapillary instabilities, Ann. Rev. Fluid Mech. 19 (1987) 403–435.
[4] Ben Hadid H., Roux B., Thermocapillary convection in long horizontal layers of low-Prandtl-number melts subject to a horizontal temperature gradient, J. Fluid Mech. 221 (1990) 77–103.
[5] Ben Hadid H., Roux B., Buoyancy- and thermocapillary-driven flows in differentially heated cavities for low-Prandtl-number fluids, J. Fluid Mech. 235 (1992) 1–36.
[6] Doi T., Koster J.N., Thermocapillary convection in two immiscible liquid layers with free surface, Phys. Fluids A 5 (1993) 1914–1927.
[7] Nepomnyashchy A.A., Simanovskii I.B., Numerical investigation of thermocapillary convection in two-layer systems, in: Hydrodynamics and Transfer Process in Microgravity, USC AS USSR, Sverdlovsk, 1983, pp. 161–166.
[8] Simanovskii I.B., Nepomnyashchy A.A., in: Convective Instabilities in Systems with Interface, Gordon and Breach, London, 1993.
[9] Pshenichnikov A.F., Tokmenina G.A., Deformation of the free surface of a liquid by thermocapillary motion, Fluid Dyn. 18 (1983) 463–465.
[10] Tan M.J., Bankoff S.G., Davis S.H., Steady thermocapilary flows of thin liquid layers, Phys. Fluids A 2 (1990) 313–321.
[11] Smith M.K., Davis S.H., Instabilities of dynamic thermocapillary liquid layers, Part 2, Surface-wave instabilities, J. Fluid Mech. 132 (1983) 145.
[12] Myznikov V.M., Finite-amplitude spatial disturbances of the advective motion in a horizontal layer with a free boundary, in: Convective Flows, Perm State Pedagogical Institute, Perm, 1981, pp. 83–88. In Russian.
[13] Smith M.K., Davis S.H., Instabilities of dynamic thermocapillary liquid layers, Part 1, Convective instabilities, J. Fluid Mech. 132 (1983) 119–144.
[14] Canright D., Thermocapillary flow near a cold wall, Phys. Fluids 6 (1994) 1415–1424.
[15] Zebib A., Homsy G.M., Meiburg E., High Marangoni number convection in a square cavity, Phys. Fluids 28 (1985) 3467–3476.
[16] Shevtsova V.M., Kuhlmann H.C., Rath H.J., Thermocapillary convection in liquid bridges with a deformed free surface, in: Ratke L., Walter H., Feuerbacher B. (Eds), Materials and Fluids under Low Gravity, Springer, 1996, pp. 323–329.
[17] Nepomnyashchy A.A., Order parameter equations for long-wavelength instabilities, Physica D 86 (1995) 90–95.
[18] Moffat H.K., Viscous and resistive eddies near a sharp corner, J. Fluid Mech. 18 (1964) 1–18.